Absorption spectroscopy at the ultimate quantum limit from single-photon states

2017 New J. Phys. 19 023013

(http://iopscience.iop.org/1367-2630/19/2/023013)

IOP Publishing New J. Phys. 19 (2017) 023013 https://doi.org/10.1088/1367-2630/aa5512

New Journal of Physics
The open access journal at the forefront of physics

Deutsche Physikalische Gesellschaft DPG
IOP Institute of Physics

Published in partnership with: Deutsche Physikalische Gesellschaft and the Institute of Physics

OPEN ACCESS

RECEIVED
22 July 2016

REVISED
15 December 2016

ACCEPTED FOR PUBLICATION
21 December 2016

PUBLISHED
2 February 2017

PAPER

Absorption spectroscopy at the ultimate quantum limit from single-photon states

R Whittaker[1], C Erven[1], A Neville[1], M Berry[2], J L O'Brien[1], H Cable[1] and J C F Matthews[1]

[1] Quantum Engineering Technology Labs, H. H. Wills Physics Laboratory and Department of Electrical & Electronic Engineering, University of Bristol, BS8 1FD, UK
[2] H. H. Wills Physics Laboratory, University of Bristol, Tyndall Avenue, Bristol, BS8 1TL, UK

E-mail: Jonathan.Matthews@Bristol.ac.uk

Keywords: quantum metrology, absorption spectroscopy, sub-Poissonian photon statistics, ultimate quantum limit

Abstract

Absorption spectroscopy is routinely used to characterise chemical and biological samples. For the state-of-the-art in laser absorption spectroscopy, precision is theoretically limited by shot-noise due to the fundamental Poisson-distribution of photon number in laser radiation. In practice, the shot-noise limit can only be achieved when all other sources of noise are eliminated. Here, we use wavelength-correlated and tuneable photon pairs to demonstrate how absorption spectroscopy can be performed with precision beyond the shot-noise limit and near the ultimate quantum limit by using the optimal probe for absorption measurement—single photons. We present a practically realisable scheme, which we characterise both the precision and accuracy of by measuring the response of a control feature. We demonstrate that the technique can successfully probe liquid samples and using two spectrally similar types of haemoglobin we show that obtaining a given precision in resolution requires fewer heralded single probe photons compared to using an idealised laser.

1. Introduction

A sample's absorption spectrum is typically measured by comparing the wavelength and intensity of incident light with the wavelength and intensity of transmitted light. However, laser spectroscopy is bound in precision by the shot-noise limit (SNL) which can ultimately limit precision in practice due to acceptable optical effects on the sample itself from the probe, including damage [1–3]. Here we demonstrate a statistical benefit to using frequency-correlated photon pairs when performing absorption spectroscopy. By using heralded single photons, there is lower fundamental noise than that of ideal laser emission of equal intensity, and in principle we can reach the so-called ultimate quantum limit in precision in absorption measurement [4]. This is advantageous in spectroscopy where the error in measurement is optical-power dependent, such as in Doppler thermometry [5, 6], and for measuring with great precision in short time intervals, while minimising photo-chemistry, such as for observing cell dynamics [2]. To show that our setup is able to surpass the SNL experimentally when probing biological samples, we use proteins that have been well-characterised in the literature—we measure the spectra of two different types of blood protein–haemoglobin bound to oxygen and haemoglobin bound to carbon monoxide—with sub-SNL precision per detected photon. Although haemoglobin does not undergo photochemistry for near-infrared light, we do use it to demonstrate the capacity to achieve a greater resolution of distinguishing two absorption features in the same sample. We support this by analysing sub-SNL performance when measuring an optical filter.

Correlated pairs of photons can be used to herald the generation of single-photons [7] which can in turn be used to measure optical transmission with precision beyond the SNL [8, 9] with optimal performance at the ultimate quantum limit in precision [4]. The increase in precision over an attenuated laser comes from the reduction of possible photon number detection outcomes for correlated photon pairs. Detecting one of the photons in each pair heralds the presence of its counterpart single probe photon—which is either absorbed or is not. By contrast, coherent and thermal sources of light contain more than vacuum and single photon

contributions, even when attenuated—this leads, at best, to Poisson distributions of the output photon-number detection statistics and error on any subsequent estimate.

The performance of various probe states have been compared using estimation theory for various types of detection schemes [4, 10–12]. Fock states $|N\rangle$ have been found to be optimal as probes since they have zero uncertainty of photon-number at the input, resulting in a minimum spread for the photon number at the output [4, 8]. Increasing N decreases uncertainty in measurement, but does not provide additional advantage in scaling. This is quantitatively similar to the sub-SNL advantage that is obtainable in entanglement-enhanced phase estimation once losses and decoherence have been accounted for [13].

Previous experiments that achieve sub-SNL precision to reduce photo-damage to samples [1, 2] equate to optical phase estimation which relies on non-classical interference via entanglement and squeezing. The quantum-enhancement pursued here is based on the sub-Poissonian statistics of single photons [8] that can be achieved equally with single photon emitters or heralded photons generated from parametric processes. This has been achieved for monochromatic absorption imaging using spatially correlated photon pairs [9]. Squeezing has been used for sub-SNL precision in two-photon absorption spectroscopy by using optical parametric oscillator (OPO) twin beams [14]. Exploiting frequency correlations, photon pairs have been used to reveal absorption spectra [15–18]—for low illumination, correlated photon pairs enable a high signal-to-noise ratio to be maintained despite increasing levels of background illumination [19]—however, these spectroscopy experiments did not achieve sub-SNL precision. To the best of our knowledge, no experiments exploring precision absorption measurements at or near the ultimate quantum limit [4] have been reported. With increased system efficiency, source brightness and extension of spectral range, the results we present open the way to practical, optimal, sub-SNL absorption spectroscopy for broad application across science and technology.

2. Methods

2.1. Precision in loss estimation

Absorption, $0 \leqslant \alpha \leqslant 1$, is determined by comparing a known input intensity $\bar{N}$ and a measured output intensity $\bar{N}' = (1 - \alpha)\bar{N}$. This is equivalent to estimating the overall loss $\alpha = 1 - (1 - \alpha_3)(1 - \alpha_2)(1 - \alpha_1)$, where photon loss occurs (i) before the sample at the source (α_1); (ii) due to absorption by the sample (α_2); (iii) after the sample during measurement (α_3). This treatment is valid, provided the combined effect of α_1 and α_3 are calibrated with high accuracy separately from α_2 (for example by removal of the measured sample). For a dilute solution, α_2 is related to the absorbance, A, of the sample through the Beer–Lambert Law, which gives an exponential attenuation depending on the molar absorption coefficient, ε, the molar concentration, c, and the distance through the sample, l: $A = \varepsilon cl = -\log_{10}[1 - \alpha_2]$ [20].

Precision in estimating α—the reciprocal of the root mean square error $\Delta\alpha$—is limited by the fundamental statistical fluctuations of the input probe due to the quantum nature of light [21]. Given ν repetitions of measurements on the output state ρ' for the output photon number, the precision for estimating α is given by $\Delta\alpha = \Delta_\rho\hat{N}/\sqrt{\nu}\bar{N}$, where $\Delta_\rho\hat{N} = \sqrt{\langle\hat{N}^2\rangle_{\rho'} - \langle\hat{N}\rangle^2_{\rho'}}$, and $\hat{N}$ is the output photon-number operator. Classical absorption spectroscopy uses laser emission as its lowest noise input probe, and so the probability to detect n photons from the input probe, $P(n)$, and n' photons after absorption, $P'(n')$, are both governed by a Poisson distribution [22]: $P(n) \mapsto P'(n') = \mathrm{e}^{-\bar{N}(1-\alpha)}[\bar{N}(1 - \alpha)]^{n'}/n'!$ This yields the fundamental limit of precision for classical light (the SNL) $\Delta\alpha_{cl} = \sqrt{(1 - \alpha)/\nu\bar{N}}$ [12]. Other incoherent broadband probe sources such as sodium lamps, and non-ideal laser setups lead to noisier intensity measurements. For a Fock state $|N\rangle$ acting as the probe, the loss process results in a binomial distribution $P'(n') = \binom{N}{n'}(1 - \alpha)^{n'}\alpha^{N-n'}$ which results in $\Delta\alpha_F = \sqrt{\alpha(1 - \alpha)/\nu\bar{N}}$ [4], an improvement of $1/\sqrt{\alpha}$ over the SNL. Note that this precision ratio is independent of $\bar{N}$. Equivalently, for a given target precision $\Delta\alpha$, a factor of α fewer single photons in the state $|1\rangle$ are needed than when using a coherent state with $\bar{N} = 1$.

We compare in figure 1 the performance of loss estimation for using the Fock state $|1\rangle$ against using an ideal laser modelled with Poisson-distributed photon-number statistics and having the same photon intensity, $\bar{N} = 1$. Performance is quantified using $\nu/\Delta^2\alpha$ which corresponds to the statistical information gained per detected photon—this is the same as the Fisher Information that is widely used in quantum parameter estimation [4, 12]. Figure 1 illustrates that in principle there is an advantage for using $|1\rangle$ for any α, however the magnitude of the improvement scales with α itself: the greatest improvement occurs at low total absorption. Since α is defined including losses throughout the system, this scheme can obtain a quantum advantage with non-perfect components. To evidence the potential for single photons to reach the ultimate quantum limit in precision in estimating absorption, we use single photons heralded from correlated photon pairs (see methods)

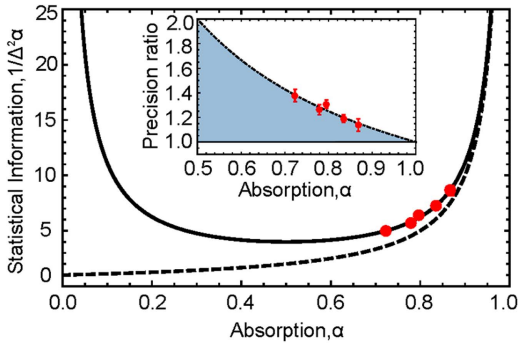

Figure 1. Theory for precision in estimating the overall loss α: use of the Fock state $|1\rangle$ is represented by the solid line (ultimate quantum limit) and use of a coherent state with the same average intensity of $\bar{N} = 1$ photons is represented by the dashed line (SNL). Note that divergence at $\alpha = 0$, 1 corresponds to estimates with vanishing variance—e.g. for $\alpha = 1$, repeated trials with $|1\rangle$ will always yield a zero-photon detection event yielding $\Delta^2\alpha = 0$. Inset: the dotted–dashed line corresponds to the ideal quantum advantage that can be obtained using $|1\rangle$, defined by the precision ratio of $\Delta^2\alpha$ for the $|1\rangle$ and a coherent state with $\bar{N} = 1$. Note that the independence of $\bar{N}$ in the precision ratio means that we would expect the same behaviour for an experiment performed with $|N\rangle$ with $N > 1$ and compared to a coherent state with the same average intensity. The data points (red) are taken at a fixed wavelength using neutral density filters in arm a to simulate loss—close agreement with the theoretical ultimate quantum limit evidences the potential for using single photons to reach the ultimate levels in precision for absorption spectroscopy. Since α is the overall absorption, the gain in precision over the SNL is limited by components such as detectors, motivating the need for increased efficiency photon-pair sources and single photons detectors. The photon source used for these data points is detailed in the appendix.

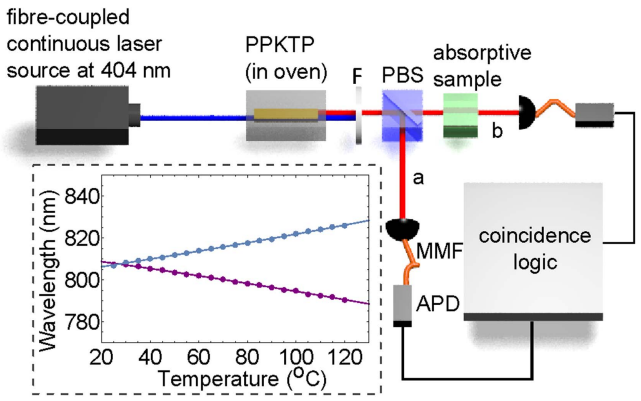

Figure 2. Setup for sub-shot-noise spectroscopy, highlighting the simplicity of the scheme. Wavelength correlated photon pairs are generated using a laser to pump a nonlinear optical crystal (PPKTP) that is phase-matched for collinear type-II SPDC and temperature tuned for wavelength control. The sample to be measured can include optical filters, cuvettes containing a liquid chemical or biological sample. PBS-polarising beamsplitter; MMF-multimode fibre; APD-avalanche photodiode; F-optical filters. Inset: the calibrated temperature dependent joint spectrum of the horizontally polarised (blue) and vertically polarised (purple) photons generated in our PPKTP crystal when pumped with a 403.9 nm continuous wave diode laser.

to estimate the total absorption α of an optical channel, where α_2 is changed with a series of neural density filters. Plotting them in figure 1, we see strong agreement with the theoretical limit.

2.2. Quantum-enhanced spectroscopy setup

Our experimental setup is shown in figure 2. A continuous wave diode laser at 403.9 nm pumps a non-linear optical crystal (periodically poled potassium titanyl phosphate, PPKTP), phase-matched for collinear type-II spontaneous parametric down conversion (SPDC). This generates pairs of orthogonally-polarised photons in the same spatial mode (H and V). The pump laser is filtered out using 3 dichroic mirrors normal to the beam that reflect 404 nm and transmit 808 nm, 2 dichroic mirrors at at 45° to the beam that reflect 808 nm and transmit 404 nm, a 715 nm longpass filter and bandpass filter centred at 810 nm (FWHM = 50 nm). This arrangement of filtering optics is represented by 'F' in figure 2. We verified that these optics removed the pump photons using a single photon sensitive spectrometer, since leaked pump photons would degrade the precision of our estimator and could lead to over exposure of the sample from un-wanted wavelengths. After filtering out the pump laser, the photons within a pair are deterministically separated using a polarising beamsplitter (PBS). The photon pairs are generated in a low gain parameter regime of SPDC and so are modelled by $|\text{SPDC}\rangle \approx |0\rangle_a|0\rangle_b + \epsilon|1\rangle_a|1\rangle_b$. An absorptive sample is placed in one path after the PBS. At the output of the experiment the photons from each

path are coupled into multimode fibres and sent through to avalanche photodiode single photons detectors (APD) with coincidence logic. The PPKTP crystal is in a temperature-tuneable oven, for a fixed laser input there is a given crystal-temperature for which the photons are degenerate. As the temperature of the crystal is changed, the phase-matching within the crystal also changes resulting in the wavelength of one photon in the pair increasing and the other decreasing—conserving energy and momentum. Using a single photon sensitive spectrometer, the crystal temperature photon wavelength relationship is precalibrated (see inset of figure 2). Once calibrated, the temperature of the crystal is tuned in order to take a spectrum. This configuration removes the need to optically determine the wavelength of either photon at the output of our setup during a sample measurement and simplifies the setup to use only two single photon detecting pixels—in our case single photon counting modules and coincidence logic.

Absorption estimates from each single probe photon are distributed across the photon's bandwidth—this is a limiting factor for both the resolution and precision of measured spectra. Here, the bandwidth of photons generated from SPDC is dependent upon that of the pump laser. We use a laser with a linewidth of 0.057 nm (FWHM) resulting in linewidths of ~0.5 nm and ~0.7 nm for the photons in arms *a* and *b* respectively. The accessible wavelength range for each arm for our setup is $773 \leqslant \lambda_a \leqslant 809$ and $806 \leqslant \lambda_b \leqslant 845$ nm, restricted by the maximum temperature of our oven (=200 °C) and our use of a fixed frequency pump laser. Each path *a* and *b* is coupled into multimode fibres to increase photon collection efficiency and to reduce sensitivity to mechanical vibrations. In the absence of a sample, the efficiency of each arm is $\eta_a \sim 35\%$ and $\eta_b = (1 - \alpha_1)(1 - \alpha_3) \sim 29\%$—this includes the ~69% specified efficiency of our single-photon detector modules that are used with coincidence logic to record both the singles count rates (N_a, N_b) and the coincidence count rates (N_{ab}).

3. Results

3.1. Sub-shot-noise spectroscopy: control feature

Figure 3 displays the application of our setup to measure the spectral response of a Gaussian bandpass filter[3] placed in path *b*. The absorption is estimated directly [23] from the ratio of heralded single photon detection events in path *a* to coincidences, according to

$$\alpha_{\text{exp}} = 1 - N_{ab}/N_a. \tag{1}$$

To take a complete spectrum, α_{exp} is calculated at a range of different crystal temperatures corresponding to a known set of wavelengths. To characterise precision for each probing wavelength we compute the mean value of $\alpha_{\text{exp}} = 1 - (1 - \alpha_1)(1 - \alpha_2)(1 - \alpha_3)$ and the variance $\Delta^2\alpha_{\text{exp}}$ over trials $\nu = 1500$ using a 1 s integration time per trial and a rate of ~800 kHz, limited by the saturation current of our detectors. For this we used a laser rated at total power 50 mW, attenuated to <1 mW. Note that the time taken to estimate an absorption spectrum using single photon states operating at the ultimate quantum limit is dependent on the brightness of the source, the number of photons required to achieve a given level of precision and the number of probing wavelengths. To ensure a stable probing wavelength after each temperature change, we enforce a 300 s stabilisation period before beginning the next set of measurements. The absorption spectrum of the filter, α_2, was found by dividing out the system absorption due to α_1 and α_3 that was characterised separately. The mean values of α_2 for each wavelength are plotted in figure 3(a) where the black dots are from our experimental setup and the black line is that from a classical scan using a UV/Vis spectrometer. Close agreement verifies comparable accuracy to commercial spectroscopy, up to 0.7 nm resolution defined by the photon bandwidth in path b. There was a uniform 0.375 nm offset between our setup and the spectrometer due to calibration discrepancy between the UV/Vis and the single-photon-sensitive spectrometers, and minor alignment error of the Gaussian filter when mounted in the UV/V is spectrometer.

The quantum advantage obtainable with our setup to measure the Gaussian filter is quantified in figure 3(b). We plot the ratio of our computed variance for the heralded single photons, compared to what we would obtain using a shot-noise limited ideal laser (solid line in the inset of figure 1), for each corresponding mean estimate of α_{exp} in figure 3(a). Of the 1500 trials we use sets of 100 to compute 15 quantum advantage parameters; the mean of these are plotted in figure 3(b) and the standard error of each mean value are plotted as the error bars. The blue region shows where a quantum advantage is obtained and the dotted–dashed line shows the maximum theoretical advantage for each α_{exp} value. A quantum advantage in precision is achieved across the range of the filter, with a maximum advantage of $22.20 \pm 0.04\%$ per detected photon.

[3] (Thorlabs FB810-10, centre wavelength 810 nm, bandwidth 10 ± 2 nm (FWHM)).

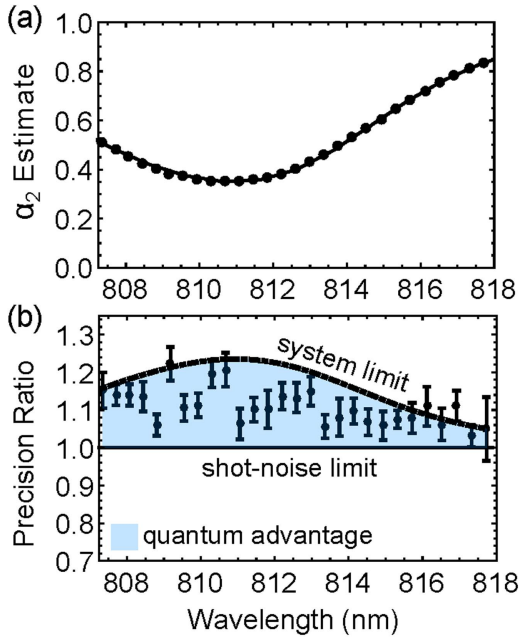

Figure 3. Sub-shot-noise absorption spectra of a control feature. A Gaussian bandpass filter was placed in arm *b* and its spectral response across the wavelength range 807–818 nm was measured with correlated photon pairs (dots) and a commercial UV/Vis spectrometer (solid line). (a) The mean absorption of the filter extracted from 1500 estimates for each measured wavelength. (b) Measured quantum advantage (data points) for estimating α of the Gaussian filter, quantified as a ratio of the precision obtainable with an ideal laser (solid line). The data was collected in sequence starting from 807 nm, moving up to 818 nm over the crystal oven temperature range from 26 degrees to 80 degrees. The system limit (dotted–dashed line) is the ultimate quantum limit for system efficiency of the current setup, accounting for α_{1-3}. Note that this system limit does not account for technical noise in our setup, that results in observed performance below the ultimate noise free limit predicted for a perfect photon pair setup—we attribute the majority of our technical noise to the drifting of alignment of the bulk optical components, limitations of temperature stability for the PPKTP crystal oven (which controls the phase matching for the downconversion crystal) and non-perfect spectral stability and finite spectral bandwidth of the emitted photons. In the current experimental setup, we were unable to quantify the individual impact of each of these sources of noise. Error bars computed as explained in the main text.

3.2. Sub-shot-noise spectroscopy: haemoglobin

To ascertain the setup can also beat the SNL in precision when probing liquid samples, we demonstrate sub-SNL spectroscopy of biological samples in the near-infrared region. We measure the absorbance spectra for two different types of haemoglobin—oxyhaemoglobin (HbO_2) and carboxyhaemoglobin (HbCO)—due to their similar spectral profiles in our accessible wavelength range. The samples were placed in path *a* and subjected to the same intensity and data integration time as when measuring the Gaussian filter. From the mean estimate for α_2, we used the Beer–Lambert law ($A = -\log_{10}[1 - \alpha_2]$) to calculate the estimated absorbance spectrum for each sample, plotted in figure 4(c). A near-flat spectrum with HbCO more absorbing than HbO_2 is obtained, as expected both from literature [24, 25] and from our own characterisation using the UV/Vis spectrometer. We plot in figures 4(a) and (b) the quantum advantage in precision of estimating the spectral profile of each sample, showing that a quantum advantage in precision per detected photon is achieved across the entire spectral range for both samples.

Fock states can be used to reduce the number of photons required to discriminate between different absorptions α, leading to a higher absorptive resolution than when using an ideal laser. We demonstrate this in figure 4(d) using the two different haemoglobin samples. Using one probe wavelength (790.5 nm) and a constant intensity, we computed α for an increasing total number of photons—we controlled this by increasing the integration time linearly starting from 1 ms, using 1 ms increments for high resolution and 5ms increments for lower resolution. For each increment we computed 800 estimates of α and calculated the mean and standard deviation $\Delta\alpha$. The standard deviation decreases with increasing total number of photons at a rate that is faster than can be obtained with an ideal laser. This is shown by the vertical lines in figure 4(d) that quantify the number of photons each scheme requires to resolve α_{HbO} from α_{HbCO} by a separation defined by multiples of the standard deviation, for our experiment (solid) and an ideal laser (dashed). The difference in total number of photons required in our scheme compared to using an ideal laser will depend on the values of α (see figure 1).

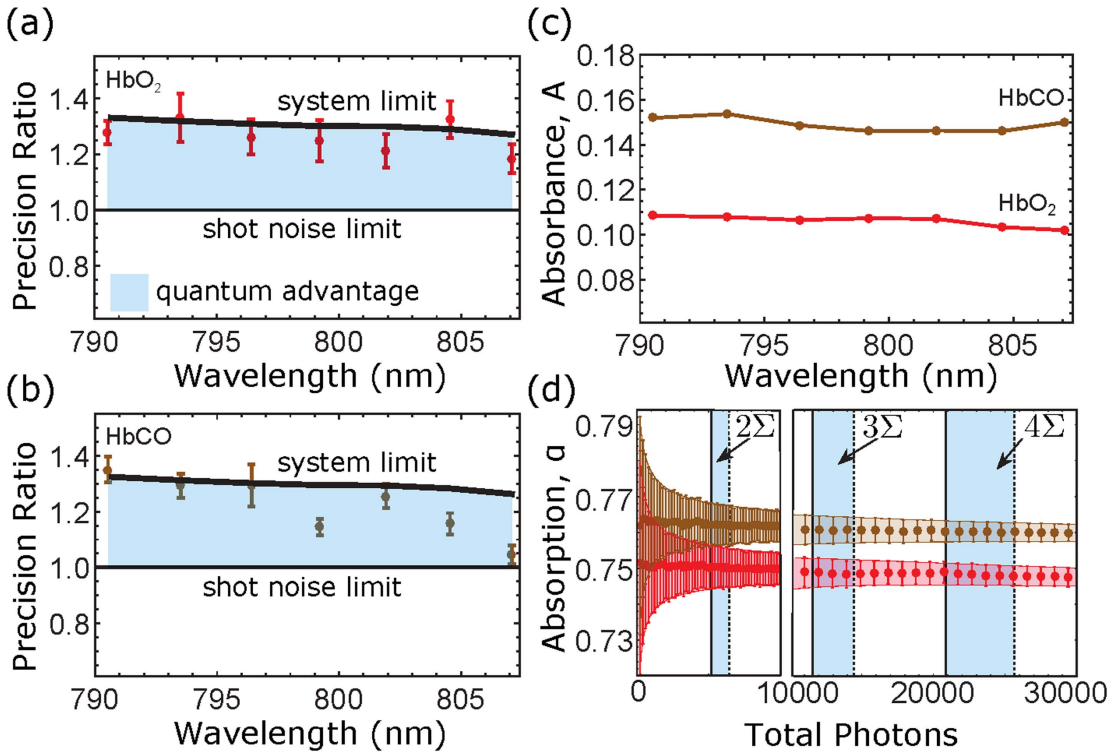

Figure 4. Sub-shot-noise absorbance spectra of HbO_2 and HbCO. Samples of HbO_2 (red) and HbCO (brown) were placed, in turn, in path *a* and the spectral response was measured over the wavelength range ~790–808 nm. The experimental quantum advantage for estimating absorption α is plotted separately for HbO_2 (a) and HbCO (b). The error bars are computed using the same treatment as for the Gaussian filter. Note that the total data in figure 3(b) exhibits an increased amount of noise, at shorter wavelengths, compared to the total set of data plotted in (a), (b) here. We attribute this to a longer total data acquisition for figure 3 due to the higher resolution measured for the gaussian filter compared to the somewhat flatter spectral response of the features reported here and the temperature of the crystal oven being set further from room temperature than the majority of data in figure 3(b). This means the data in figure 3(b) is subject to increased sources of technical noise with time. The 7 data points in each of (a), (b) here take the same collective time as the 7 data points collected at the highest crystal oven temperature of figure 3 which agrees with the observation that these sets of data exhibit comparable levels of noise. (c) The mean value of α measured with our system was converted to absorbance of the sample, $A = -\log_{10}(1-\alpha_2)$, accounting for characterised system efficiency $(1-\alpha_1)(1-\alpha_3)$. This enables for direct comparison to previously reported spectral measurements [24, 25], to which we find close agreement. (d) Resolving α_{HbO} from α_{HbCO} at 790.5nm probe wavelength. For each total number of photons, 800 estimates for α are made and the mean is plotted (circles). The error on these estimates is quantified by one standard deviation ($\Delta\alpha$) of these estimates and plotted as error bars. Solid black vertical lines represent the total number of photons detected in our experiment and required to resolve the absorbance of HbCO from the absorbance of HbO_2 from each other by quantities 2Σ, 3Σ and 4Σ, where Σ is the average of one standard deviation of the estimate of α for HbCO and one standard deviation of the estimate of α for HbO_2 using the associated ν trails—these vertical lines are computed by fitting curves that scale with $1/\sqrt{\nu}$ to the error bars for each sample, due to the independence of one trial to the next. We compare this directly to the total number of photons required to resolve the two α when using an ideal laser (vertical dashed lines). The shaded regions (left to right) correspond to 1250, 2850 and 4810 fewer required photons. We performed a high resolution scan (1ms increments) for the region of 2Σ separation. Because the precision ratio plotted in (a) and (b) is dependent upon the total transmission of the photon pair source $1-\alpha$, we have plotted absorption in panel (d) in terms of α. Details of synthesising the two types of haemoglobin in detailed in the appendix.

4. Discussion

In this work, we have studied the information obtainable from performing absorption measurement with Fock states of the case of $N = 1$ and compared it to the performance of a coherent state of intensity $\bar{N} = 1$. Of course, increasing intensity $\bar{N}$ for coherent states is relatively straightforward in practice, which enables an increase in precision. We feel that the evidence reported here provides compelling motivation to overcome the difficulty associated in creating on-demand larger Fock states of $N > 1$ photons. But we note that even performing few-photon quantum metrology has predicted benefits for application in biology where the number of photons in a given optical probe is limited [26] and intensity cannot be continually increased to obtain greater precision.

Strategies using squeezed vacuum states, which can readily be produced by an OPO, have been shown to be optimal in the limit of very low absorption and low probe intensity [4, 12]—and experimentally large gains have been shown in this regime [11]. Although the OPO can achieve high intensities using these probe states, this it at the cost of sub-optimal behaviour across the entire range of α, including $\alpha = 0$ [12]. More generally, any source of squeezed light generates quantum states which correspond mathematically to displacement and squeezing operators acting on thermal states (including the vacuum), and the precision achievable with these probe states was studied in [12]. As shown in [4], general squeezed states are sub-optimal other than when $\alpha \to 0,\ 1$—with

this remaining true irrespective of the detection method used (e.g. homodyne detection or photon number counting). In contrast, Fock state probes together with photon-number counting measurements are optimal for any α and probe intensity.

The focus of quantum metrology literature has been on demonstrating physical principles of quantum metrology, with only a few recent examples starting to work with samples and moving towards quantifying sample damage [1, 3, 27]. While the haemoglobin used here is not photo-sensitive, it was important to show that our setup can still beat the SNL when probing chemical/biological samples. HbCO and HbO_2 were suitable candidates because their distinct spectral features in the range 450–650 nm [24, 25] meant their successful synthesis could be confirmed while their very similar spectral responses in the range 790–840 nm enabled us to demonstrate the higher absorptive resolution that can be achieved using Fock states for absorption spectroscopy. Future work will include probing samples that would benefit from low-light exposure.

Unlike other demonstrations in quantum-enhanced precision measurement, our setup does not require entanglement or multi-photon interference. The quantum-advantage in precision arises due to the binomial statistics gained using heralded Fock states. Since Fock states with $N > 1$ also have binomial statistics, the statistical advantage is equivalent, but unlike phase estimation experiments, not improved. Equivalent performance could be obtained with extremely narrow bandwidth single photons generated from quantum dots [28, 29] or atom-cavity systems [30]. Proposed characterisation of photon-counting and homodyne detectors with Fock states [31] could use an iteration of our setup to benchmark spectral response.

5. Conclusions

We have demonstrated a promising new branch of spectroscopy—correlated photon pair absorption and absorbance spectroscopy for sub-SNL precision, approaching the ultimate quantum limit [4]. There are four main aspects of our setup where performance can be improved. (i) Increasing overall system efficiency will enable a greater quantum advantage (figure 1) due to the statistical benefit arising from estimating the total loss —superconducting detectors are a promising approach, >90% efficiency have been demonstrated at telecommunication wavelengths [32] with promise of high efficiency at shorter wavelengths [33]; high efficiency single-photon-sensitive cameras [9] could be applied alleviating the need for cryogenic temperatures. Increased overall system efficiency will also enable experimental test of the precision obtainable in practice with Fock states over a greater controlled range of α, shown in figure 1. (ii) Extending emission to a larger spectral range would increase application—this can be accomplished with a tuneable pump laser [34] or the use of a broadband source together with spectral analysis on the heralding arm. (iii) Generating photons with narrow bandwidths would enable higher spectral resolution—for example, cavity-enhancement [1] would enable application to atomic spectroscopy, where bandwidths of 0.01–0.001 nm are required [35]. Producing spectrally narrower photons increases their coherence length, which reduces the fundamental limit on the rate at which individual photon pairs can be detected using single photon APDs due to the increased potential for overlap of arrival time. For the spectral bandwidth and range used in this experiment, this limit is ~300 GHz, while for bandwidths necessary for atomic spectroscopy this limit would be of order 500 MHz. By replacing the APDs with number resolving detection—through, for example, multiplexing APDs [36] or using superconducting transition edge sensors [37, 38]—this limit on the photon pair production rate is circumvented. (iv) Increasing photon-pair production rate using longer PPKTP crystals both increases source brightness and reduces the spectral bandwidth of the photon pairs [39]. Another alternative would be to use sources based on an optical parametric amplifier [40] together with number resolving detection.

Likely applications include characterising samples that are photo-sensitive to the optical probe [41–43]. Furthermore, our technique would be advantageous for probing samples of low concentration or volume—the principle demonstrated in figure 4(d) applied to neighbouring points on a single spectrum, demonstrates the advantage when probing shallow spectral features.

Acknowledgments

The authors would like to thank R Oulton, A Young, P Androvitsaneas, S Carswell, B Lang and E Harbord for use of the spectrometer; S Bellamy, P Dunton and M Mercer for wet-lab support; G Magro for materials-lab support; X Q Zhou, J Rarity, M Padgett, A Datta, for useful discussions; N Tyler, A Santamato and C Wilkes for preliminary work on the source. Funding: the authors are grateful for support from DSTL, EPSRC, ERC. AN is grateful for support from the Wilkinson Foundation. JLOB acknowledges a Royal Academy of Engineering Chair in Emerging Technologies and a Wolfson Merit Award. JCFM is supported by an EPSRC Early Career Fellowship. Author Contributions: RW constructed/performed experiment, analysed data, prepared the haemoglobin samples; CE constructed experiment and part-wrote counting software for filter work; AN wrote

counting software for haemoglobin work; MB prepared the haemoglobin samples; JLOB conceived the experiment, HC constructed the theory, JCFM conceived and designed the experiment. All authors contributed to the writing the manuscript. Competing interests: the authors declare that they have no competing interests. Data and material availability: all data needed to evaluate the conclusions in the paper are presented graphically in the paper. Underlying data are openly available under the doi: 10.5523/bris.1g55e0oh0sl6v1tzztdrbeullo.

Appendix

A.1. Photon source used for figure 1

The data taken in figure 1 was with an updated version of the source described above. The setup is very similar—the same laser was used, but fewer components and mounted into a cage-system. The fibre coupled laser is passed through a narrow bandpass filter (central wavelength 404 nm) and a PBS. The pump is focused onto a 30 mm PPKTP crystal, and filtered out using one wide bandpass filter and one longpass filter. The photons are spatially separated using a PBS before coupling into single-mode fibre at the output.

A.2. Preparation of oxy- and carboxyhaemoglobin

A.2.1. Oxyhaemoglobin. We converted methaemoglobin (Bovine, lyophilised powder, Sigma Aldrich, H2500) to oxyhaemoglobin (reduced) using a procedure based on both Sigma Aldrich and [44]. A 30 $\times$ 1 cm Sephadex G-25 column was equilibrated with 20 mM phosphate buffer (pH 7.0) containing 10–3 M EDTA. 200 mg ml^{-1} sodium dithionite was added to 1 ml buffer and applied to the column, followed by a further 1 ml buffer and 5 ml methaemoglobin (20 mg ml^{-1}). A colour change brown to red was observed as the haemoglobin reached the sodium dithionite. The reduced haemoglobin was dialysed against oxygen-saturated buffer, with oxygen continually bubbling into it. Dialysis was carried out for 2 $\times$ 30 min, with one buffer change. Half of this oxyhaemoglobin was used for preparing carboxyhaemoglobin.

A.2.2. Carboxyhaemoglobin. We used the much higher affinity of haemoglobin for carbon monoxide [45] to prepare carboxyhaemoglobin, by directly bubbling carbon monoxide into the oxyhaemoglobin for 5 min.

References

[1] Wolfgramm F, Vitelli C, Beduini F A, Godbout N and Mitchell M W 2013 *Nat. Photon.* **7** 28
[2] Taylor M A, Janousek J, Daria V, Knittel J, Hage B, Bachor H-A and Bowen W P 2013 *Nat. Photon.* **7** 229
[3] Taylor M A and Bowen W P 2016 *Phys. Rep.* **615** 1–59
[4] Adesso G, Dell'Anno F, De Siena S, Illuminati F and Souza L A M 2009 *Phys. Rev.* A **79** 040305R
[5] Stace T and Luiten A 2010 *Phys. Rev.* A **81** 033848
[6] Stace T M, Truong G-W, Anstie J, May E F and Luiten A N 2012 *Phys. Rev.* A **86** 012506
[7] Grangier P, Roger G and Aspect A 1986 *Europhys. Lett.* **1** 173
[8] Jakeman E and Rarity J G 1986 *Opt. Commun.* **59** 219
[9] Brida G, Genovese M and Rou Berchera I 2010 *Nat. Photon.* **4** 227
[10] Hayat M M, Joobeur A and Saleh B E A 1999 *J. Opt. Soc. Am.* A **16**
[11] D'Auria V, de Lisio C, Porzio A, Solimeno S and Paris M G A 2006 *J. Phys. B: At. Mol. Opt. Phys.* **39** 1187
[12] Monras A and Paris M G A 2007 *Phys. Rev. Lett.* **98** 160401
[13] Escher B, de Matos Filho R and Davidovich L 2010 *Nat. Phys.* **7** 406
[14] Ribeiro P H S, Schwob C, Maître A and Fabre C 1997 *Opt. Lett.* **22** 1893
[15] Scarcelli G, Valencia A, Gompers S and Shih Y 2003 *Appl. Phys. Lett.* **83** 5560
[16] Kalachev A A, Kalashnikov D A, Kalainkin A A, Mitrofanova T G, Shkalikov A V and Samartsev V V 2008 *Laser Phys. Lett.* **5** 600
[17] Slattery O, Ma L, Kuo P, Kim Y S and Tang X 2013 *Laser Phys. Lett.* **10** 075201
[18] Yabushita A and Kobayashi T 2004 *Phys. Rev.* A **69** 013806
[19] Kalachev A A, Kalashnikov D A, Kalainkin A A, Mitrofanova T G, Shkalikov A V and Samartsev V V 2007 *Laser Phys. Lett.* **4** 722
[20] Atkins P and de Paula J 2014 *Atkins' Physical Chemistry* 10th edn (Oxford: Oxford University Press)
[21] Giovannetti V, Lloyd S and Maccone L 2004 *Science* **306** 1330
[22] Scully M O and Zubairy M S 2014 *Quantum Optics* (Cambridge: Cambridge University Press)
[23] Brida G, Genovese M and Novero C 2000 *J. Mod. Opt.* **47** 2099
[24] Zijlstra W, Buursma A and Meeuwsen-Van der Roest W 1991 *Clin. Chem.* **37** 1633–8 (http://clinchem.aaccjnls.org/content/37/9/1633)
[25] Zijlstra W and Buursma A 1997 *Comparative Biochem. Physiol.* B **118** 743
[26] Taylor M A and Bowen W P 2016 *Phys. Rep.* **615** 1
[27] Phan N M, Cheng M F, Bessarab D A and Krivitsky L A 2014 *Phys. Rev. Lett.* **112** 1
[28] Young R, Stevenson R, Shields A, Atkinson P, Cooper K and Ritchie D 2007 *J. Appl. Phys.* **101** 081711
[29] Jayakumar H, Predojevic A, Huber T, Kauten T, Solomon G and Weihs G 2013 *Phys. Rev. Lett.* **110** 135505
[30] Kuhn A, Hennrich M and Rempe G 2002 *Phys. Rev. Lett.* **89** 067901
[31] Barbieri M, Datta A, Bartley T J, Jin X-M, Kolthammer W S and Walmsley I A 2016 *Quant. Meas. Quant. Metrol.* **3** 9–14
[32] Marsili F *et al* 2013 *Nat. Photon.* **7** 210
[33] Marsili F, Bellei F, Najafi F, Dane A, Dauler E, Molnar R and Berggren K 2012 *Nano Lett.* **12** 4799
[34] Jin R-B, Shimizu R, Wakui K, Benichi H and Sasaki M 2013 *Opt. Express* **21** 10659

[35] Andrade-Garda J M 2013 *Basic Chemometric Techniques in Atomic Spectroscopy* (Cambridge: Royal Society of Chemistry)
[36] Achilles D, Silberhorn C, Sliwa C, Banaszek K, Walmsley I A, Fitch M J, Jacobs B C, Pittman T B and Franson J D 2004 *J. Mod. Opt.* **51** 1499
[37] Miller A J, Nam S W, Martinis J M and Sergienko A V 2003 *Appl. Phys. Lett.* **83** 791
[38] Fukuda D *et al* 2011 *Opt. Express* **19** 870
[39] Fedrizzi A, Herbst T, Poppe A, Jennewein T and Zeilinger A 2007 *Opt. Express* **15** 15377
[40] Cooper M, Wright L J, Söller C and Smith B J 2013 *Opt. Express* **21** 5309
[41] Puppels G, Olminkhof J, Segers-Nolten G, Otto C, de Mul F and Greve J 1991 *Exp. Cell Res.* **195** 361
[42] Carlton P M *et al* 2010 *Proc. Natl Acad. Sci.* **107** 16016
[43] Barroso Peña Á, Kemper B, Woerdemann M, Vollmer A, Ketelhut S, von Bally G and Denz C 2012 *Proc. SPIE* **8427** 84270A
[44] Dixon H B F and McIntosh R 1967 *Nature* **213** 399
[45] Blumenthal I 2001 *J. R. Soc. Med.* **94** 270–2 (www.ncbi.nlm.nih.gov/pmc/articles/PMC1281520/)